# Heavy Particle Clustering in Inertial Subrange of High–Reynolds Number Turbulence

Keigo Matsuda,[1,*] Katsunori Yoshimatsu,[2] and Kai Schneider[3]
[1]Research Institute for Value-Added-Information Generation (VAiG), Japan Agency for Marine-Earth Science and Technology (JAMSTEC), Yokohama 236-0001, Japan
[2]Institute of Materials and Systems for Sustainability, Nagoya University, Nagoya, 464-8601, Japan
[3]Institut de Mathématiques de Marseille (I2M), Aix-Marseille Université, CNRS, 13331 Marseille Cedex 3, France

(Received 4 February 2024; accepted 6 May 2024; published 3 June 2024)

Direct numerical simulation of homogeneous isotropic turbulence shows pronounced clustering of inertial particles in the inertial subrange at high Reynolds number, in addition to the clustering typically observed in the near dissipation range. The clustering in the inertial subrange is characterized by the bump in the particle number density spectra and is due to modulation of preferential concentration. The number density spectrum can be modeled by a rational function of the scale-dependent Stokes number.

DOI: 10.1103/PhysRevLett.132.234001

Inertial heavy particles suspended in turbulence are frequently observed in geophysical and industrial flows, such as cloud droplets and volcanic ash in atmospheric turbulence, dust particles in protoplanetary disks, and fuel droplets in spray combustion. The particles show nonuniform distribution, i.e., clustering, in turbulence due to deviation of particle motion from the fluid motion [1–3]. Clustering of inertial heavy particles has been studied extensively; for reviews we refer to, e.g., Refs. [4–8]. The clustering can be characterized statistically by two-point correlation of number densities such as the radial distribution function (RDF) and the number density spectrum. The former is relevant to, e.g., droplet collision and coalescence statistics in raindrop formation process [9,10], and the latter gives estimates of clustering influence on cloud radar reflectivity factor [11,12]. The mechanism of the clustering is explained by the preferential concentration in the pioneering work by Maxey [1] when the particle relaxation time $\tau_p$ is sufficiently smaller than the flow timescale: inertial particles are swept out from turbulent vortices due to the centrifugal effect and concentrate in low vorticity and high strain-rate regions. The inertial effect can be quantified by the Stokes number defined as $\mathrm{St} \equiv \tau_p/\tau_\eta$ with the Kolmogorov time $\tau_\eta \equiv \sqrt{\nu/\epsilon}$. Here, $\nu$ is the kinematic viscosity, and $\epsilon$ is the mean energy dissipation rate per unit density. The review [7] well summarizes clustering mechanisms including other ones proposed for larger $\tau_p$.

Inertial particles show multiscale clustering structures [13–19], whose number density spectrum has a pronounced bump in the near dissipation range, i.e., the scales between the inertial and dissipation ranges [11]. The closure analysis in Ref. [18] predicted a universal scaling for the number density fluctuation in the inertial subrange. To observe such inertial subrange clustering, one needs sufficiently high–Reynolds number turbulence so that the spectrum of fluid velocity and pressure obeys the scaling based on Kolmogorov's idea [20] (K41), according to the theories in Refs. [17,18]. The recent development of supercomputers enables us to explore the influence of the Reynolds number on the clustering by using direct numerical simulation (DNS) of particle-laden turbulence. In this Letter, we examine the inertial subrange clustering and its dependence on the Stokes number by performing three-dimensional DNS at high Reynolds number.

We consider statistically homogeneous turbulent flow governed by the incompressible Navier-Stokes (NS) equation, $\partial \boldsymbol{u}/\partial t + \boldsymbol{u}\cdot\nabla\boldsymbol{u} = -\nabla\mathcal{P} + \nu\nabla^2\boldsymbol{u} + \boldsymbol{f}$, where the velocity $\boldsymbol{u}(\boldsymbol{x}, t)$ satisfies $\nabla\cdot\boldsymbol{u} = 0$. Pressure per density is denoted by $\mathcal{P}(\boldsymbol{x}, t)$, and $\boldsymbol{f}(\boldsymbol{x}, t)$ is an external solenoidal forcing. We use a cubic domain with length $2\pi$ and periodic boundary conditions. The particle size is assumed to be sufficiently smaller than the Kolmogorov length $\eta \equiv (\nu^3/\epsilon)^{1/4}$, and $\rho_p/\rho \gg 1$, where $\rho_p$ and $\rho$ are the particle and fluid densities, respectively. Then, the Lagrangian motion of inertial heavy particles is governed by $d\boldsymbol{x}_p/dt = \boldsymbol{v}_p$ and $d\boldsymbol{v}_p/dt = -\{\boldsymbol{v}_p - \boldsymbol{u}(\boldsymbol{x}_p)\}/\tau_p$, where $\boldsymbol{x}_p$ and $\boldsymbol{v}_p$ are the position and velocity of a Lagrangian particle, respectively [3]. The Taylor-microscale Reynolds number is defined as $\mathrm{Re}_\lambda \equiv u'\lambda/\nu$, where $u' \equiv \sqrt{\langle|\boldsymbol{u}|^2\rangle/3}$ is the turbulent velocity fluctuation, and $\lambda \equiv \sqrt{15\nu u'^2/\epsilon}$ is the Taylor microscale. Here, $\langle\cdot\rangle$ denotes an ensemble average. A series of DNS computations of particle-laden turbulence was performed using the same numerical code as in Refs. [11,12,21,22]. External solenoidal forcing was applied at large scale, $|\boldsymbol{k}| < 2.5$, where $\boldsymbol{k}$ is the wave number vector, to obtain statistically stationary turbulence, following a random forcing scheme in Ref. [23] (see details in the Supplemental

 

TABLE I. DNS parameters and statistics of obtained turbulence; the number of grid points $N_g$, the number of particles $N_p$, the Reynolds number of DNS, $\mathrm{Re} = U_0 L_0/\nu$, $\mathrm{Re}_\lambda$, $u'$, $\epsilon$, and $k_{\max}\eta$, where $k_{\max} \equiv N_g/2$ is the maximum wave number, and $U_0$ and $L_0$ are unity.

| $N_g$ | $N_p$ | Re | $\mathrm{Re}_\lambda$ | $u'$ | $\epsilon$ | $k_{\max}\eta$ |
|---|---|---|---|---|---|---|
| 512 | $1.5 \times 10^7$ | 816 | 155 | 0.97 | 0.451 | 2.05 |
| 1024 | $5.0 \times 10^7$ | 2052 | 251 | 0.97 | 0.438 | 2.07 |
| 2048 | $4.0 \times 10^8$ | 5257 | 402 | 0.96 | 0.417 | 2.07 |
| 4096 | $3.2 \times 10^9$ | 13 212 | 648 | 0.99 | 0.453 | 2.03 |

Material [24]). Inertial particles were seeded uniformly and randomly in the turbulent flow at a statistically steady state, defined as $t = 0$. Particle position data were then sampled at 10 time instants of $t = 11T_0$ to $20T_0$ at interval of $T_0$, where $T_0$ is the dimensionless time unit, comparable to the large-eddy turnover time. Spectra in this Letter are averaged for the data at the sampling time instants. The DNS parameters and the turbulent flow statistics are summarized in Table I. The ensemble average for the statistics is computed as spatial and temporal average. The latter is taken for the period of $10T_0 \le t \le 20T_0$. The Stokes number St is 0.05, 0.1, 0.2, 0.5, 1.0, 2.0, and 5.0.

Figure 1(a) shows kinetic energy spectra $E_u(k)$ for the different flows listed in Table I. Here, $E_u(k) \equiv (1/2)\sum_k' |\hat{\boldsymbol{u}}(\boldsymbol{k})|^2$, where $\hat{\cdot}$ denotes the Fourier transform, $\sum_k' \equiv (4\pi k^2/N_k)\sum_{k-1/2\le|\boldsymbol{k}|<k+1/2}$, and $N_k$ is the number of $\boldsymbol{k}$ that satisfy $k - 1/2 \le |\boldsymbol{k}| < k + 1/2$. In the largest Reynolds number case, $\mathrm{Re}_\lambda = 648$, the compensated spectrum is nearly flat for about one decade in $k\eta$, indicating that the spectrum is close to the scaling $k^{-5/3}$ [20]. According to the preferential concentration mechanism [1,2], the clustering formation is affected by the vorticity and strain rate distributions represented by the second invariant $Q$ of the fluid velocity gradient tensor, where $Q \equiv [\boldsymbol{\Omega}:\boldsymbol{\Omega} - \mathbf{S}:\mathbf{S}]/2$ with $\boldsymbol{\Omega} \equiv [\nabla\boldsymbol{u} - (\nabla\boldsymbol{u})^T]/2$ and $\mathbf{S} \equiv [\nabla\boldsymbol{u} + (\nabla\boldsymbol{u})^T]/2$. $Q$ satisfies the relationship $2Q = \nabla^2\mathcal{P}$. The superscript $T$ denotes the transposed. Positive and negative $Q$ indicate rotation- and strain-dominated regions, respectively.

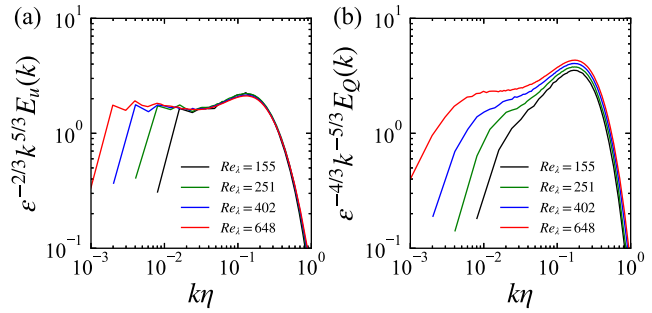


FIG. 1. (a) Compensated kinetic energy spectra and (b) compensated spectra of $Q$.

According to dimensional analysis [25–27] following K41, the spectrum of $Q$, defined as $E_Q(k) \equiv \sum_k' |\hat{Q}(\boldsymbol{k})|^2$, has a $k^{5/3}$ scaling in the turbulence inertial subrange at sufficiently high–Reynolds number because $E_Q(k)$ is equivalent to $(1/4)k^4 E_{\mathcal{P}}(k)$, where $E_{\mathcal{P}}(k) \equiv \sum_k' |\hat{\mathcal{P}}(\boldsymbol{k})|^2$ is the pressure spectrum. Figure 1(b) shows the spectra $E_Q(k)$. This figure confirms that, for $\mathrm{Re}_\lambda = 648$, the compensated spectrum is almost flat for $0.008 \lesssim k\eta \lesssim 0.03$, implying that $E_Q(k)$ well obeys the prediction of the dimensional analysis. For $\mathrm{Re}_\lambda = 648$, the forcing is imposed in $|\boldsymbol{k}|\eta < 2.48 \times 10^{-3}$, which is smaller than the above wave number range.

Spatial distributions of particles obtained by the DNS for $\mathrm{Re}_\lambda = 648$ are displayed in Fig. 2. For $\mathrm{St} = 0.05$ and 0.2, small voids distribute intermittently, whereas for $\mathrm{St} = 1.0$ and 5.0, particle nonuniformity is significant even for scales larger than $200\eta$.

We consider the particle number density field $n(\boldsymbol{x}, t)$ in the continuous setting [1] to define the particle number density spectrum $E_n(k) \equiv \sum_k' |\hat{n}(\boldsymbol{k})|^2$. To compute the spectrum, the discrete particle position data are converted into number density field data on $N_g^3$ equidistant grid points with the histogram method. The number density field is normalized such that the mean value yields $\langle n \rangle = 1$. The discrete nature of particles causes Poisson noise, and the conversion to the field data causes the suppression for large wave numbers [28]. These effects have been removed from the obtained spectra (see the Supplemental Material [24]).

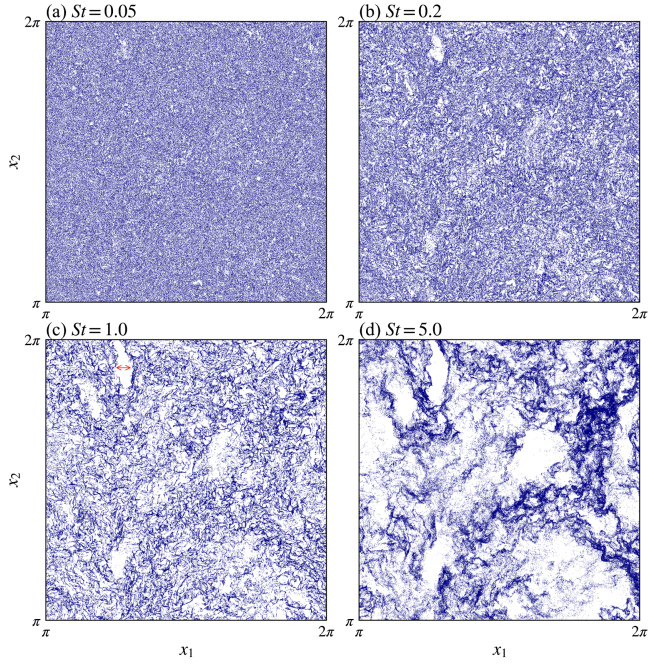


FIG. 2. Spatial distributions of the particles for (a) $\mathrm{St} = 0.05$ (b) 0.2, (c) 1.0, and (d) 5.0 at $t = 11T_0$ in the ranges of $\pi \le x_1 \le 2\pi$, $\pi \le x_2 \le 2\pi$, and $0 \le x_3 \le 4\eta$ for $\mathrm{Re}_\lambda = 648$. The red arrow in (c) indicates the length $200\eta$.

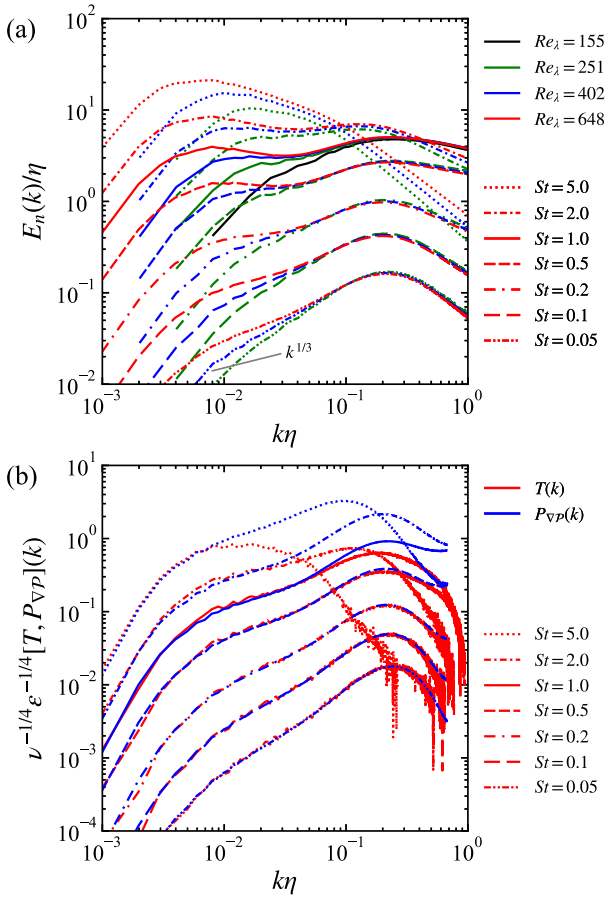


FIG. 3. (a) Particle number density spectra $E_n(k)$ for $\mathrm{Re}_\lambda = 155$, 251, 402, and 648 and (b) transfer spectra $T(k)$ for $\mathrm{Re}_\lambda = 648$ with the approximated production spectra $P_{\nabla\mathcal{P}}(k)$. The number density spectra compensated by the scaling $k^{1/3}$ are provided in the Supplemental Material [24].

Figure 3(a) shows $\mathrm{Re}_\lambda$ dependence of the number density spectra $E_n(k)$ for different St values. For $\mathrm{St} = 1.0$, each spectrum for $\mathrm{Re}_\lambda > 200$ shows a peak around $k\eta \approx 0.2$. The peak wave number of the bump near the dissipation range is similar for $\mathrm{St} \leq 1$. These observations are consistent with the results in Ref. [11]. For $k\eta \lesssim 0.03$, the spectrum values increase as $\mathrm{Re}_\lambda$ increases for all St cases, and each spectrum for $\mathrm{St} \geq 0.5$ clearly displays a bump for $\mathrm{Re}_\lambda = 648$. For $\mathrm{St} = 5.0$, only the bump for $k\eta \lesssim 0.03$ exists, and the peak near the dissipation range disappears. Note that we confirmed that the existence of the bump for $k\eta \lesssim 0.03$ is robust against the external forcing schemes [21,23] (See the Supplemental Material [24] and Ref. [29] therein). We can also observe that the slope of the spectra in the inertial subrange ($0.008 \lesssim k\eta \lesssim 0.03$) is dependent on St in contrast to the prediction by Ariki *et al.* [18], in which $E_n(k) \propto k^{1/3}$. The slope for $\mathrm{St} = 0.05$ and $\mathrm{Re}_\lambda = 648$ is close to $1/3$. However, the negative slopes for $\mathrm{St} \geq 0.5$ are obviously different from the prediction.

To examine the clustering mechanism in the inertial subrange, we consider the particle velocity field $\boldsymbol{v}(\boldsymbol{x}, t)$ in the continuous setting based on the approximation by Maxey [1], i.e.,

$$\boldsymbol{v} = \boldsymbol{u} - \tau_p \boldsymbol{a}_L + \mathcal{O}(\tau_p^2), \tag{1}$$

where $\boldsymbol{a}_L \equiv \partial\boldsymbol{u}/\partial t + \boldsymbol{u}\cdot\nabla\boldsymbol{u}$, which is the Lagrangian acceleration of fluid. Then, the conservation equation of $n$ reads $\partial n/\partial t + \nabla\cdot(n\boldsymbol{v}) = 0$. This approximation is valid at least for a coarse-grained field of $\boldsymbol{v}_p$ for a spatial scale $r$ satisfying $\tau_p \ll \tau_r$, where $\tau_r$ is the timescale of the fluid flow for $r$. Note that Maxey [1] considered the Lagrangian transport of $n$ along the inertial particle trajectory, $\partial n/\partial t + \boldsymbol{v}\cdot\nabla n = -n\nabla\cdot\boldsymbol{v}$, and applied Eq. (1) to the particle velocity divergence, yielding $\nabla\cdot\boldsymbol{v} = 2\tau_p Q + \mathcal{O}(\tau_p^2)$. The preferential concentration mechanism is explained by this approximation: the inertial particles preferentially concentrate in flow regions where $Q$ is small or negative. The conservation equation can be rewritten in the form of Lagrangian transport of $n$ along the fluid particle trajectory,

$$\frac{\partial n}{\partial t} + \boldsymbol{u}\cdot\nabla n = -\nabla\cdot(n\boldsymbol{v} - n\boldsymbol{u}), \tag{2}$$

in which the production term on the right-hand side represents the effect of particle drift velocity. Based on the advection term, $A(\boldsymbol{x}) \equiv \boldsymbol{u}\cdot\nabla n$, in Eq. (2), the transfer spectrum for the number density is defined as $T(k) \equiv 2\sum_k' \Re[\hat{A}(\boldsymbol{k})\hat{n}^*(\boldsymbol{k})]$, which represents the scale-to-scale transfer of number density fluctuation. Here, $\Re[\cdot]$ denotes the real part and the asterisk the complex conjugate. Figure 3(b) shows the transfer spectra $T(k)$ computed for each St for $\mathrm{Re}_\lambda = 648$. For all the Stokes numbers, $T(k)$ exhibits positive values in the inertial range, indicating that the forward transfer of particle number density fluctuation (from large scales to small scales) is dominant. Thus, the bump of $E_n(k)$ for $k\eta \lesssim 0.03$ is due to pronounced clustering production in the inertial range and not due to backward transfer from the dissipation range.

We analyze the clustering production in the inertial subrange based on the production term, $B(\boldsymbol{x}) \equiv -\nabla\cdot(n\boldsymbol{v} - n\boldsymbol{u}) = \tau_p\nabla\cdot(n\boldsymbol{a}_L) + \mathcal{O}(\tau_p^2)$, in Eq. (2). When considering the Fourier transform $\hat{B}(\boldsymbol{k})$ in the inertial subrange, the effect of viscosity and forcing terms on $\boldsymbol{a}_L$ is negligibly small according to the K41 phenomenology. Therefore, we can assume that only the pressure gradient term in the NS equation affects the inertial particle drift, i.e., $\hat{B}(\boldsymbol{k}) \approx \widehat{B_{\nabla\mathcal{P}}}(\boldsymbol{k})$, where $B_{\nabla\mathcal{P}}(\boldsymbol{x}) \equiv -\tau_p\nabla\cdot(n\nabla\mathcal{P})$. Then we can define the approximated production spectrum $P_{\nabla\mathcal{P}}(k) \equiv 2\sum_k' \Re[\widehat{B_{\nabla\mathcal{P}}}(\boldsymbol{k})\hat{n}^*(\boldsymbol{k})]$. Note that the exact production spectrum is equivalent to $T(k)$ assuming statistical stationarity. Figure 3(b) shows the approximated spectra $P_{\nabla\mathcal{P}}(k)$. For $\mathrm{St} \leq 2.0$, $P_{\nabla\mathcal{P}}(k)$ well agrees with $T(k)$ for $k\eta \lesssim 0.03$, including the inertial subrange. For $\mathrm{St} = 5.0$, $P_{\nabla\mathcal{P}}(k)$ and $T(k)$ show significant difference in the inertial subrange,

indicating a breakdown of the approximation (1) due to large $\tau_p$. Therefore, we can conclude that $B_{\nabla\mathcal{P}}$ plays a dominant role for the clustering production for $k\eta \lesssim 0.03$ and $\mathrm{St} \leq 2.0$, as predicted above.

The approximated production term $B_{\nabla\mathcal{P}}$ represents the production due to the convergence of the inertial particle drift, and can be rewritten as $B_{\nabla\mathcal{P}} = B_Q + B_\theta$, where $B_Q \equiv -2\tau_p Q$ and $B_\theta \equiv -\tau_p \nabla\cdot(\theta\nabla\mathcal{P})$ with $\theta \equiv n-1$, where $\langle\theta\rangle = 0$. The term $B_Q$ represents the preferential concentration mechanism, and its contribution can be dominant when the number density is nearly uniform. $B_{\nabla\mathcal{P}}$ guarantees the conservation of $n$ but $B_Q$ does not. Hence the residual term $B_\theta$ can be considered as the modification of the clustering production for the conservation of $n$. The effect of $B_\theta$ can be significant reflecting the nonuniformity of $n$.

We examine the scale dependence of the number density, transfer and production spectra in the approximated balance equation $\partial E_n(k)/\partial t + T(k) = P_{\nabla\mathcal{P}}(k)$, using dimensional analysis. Ariki *et al.* [18] predicted a scale similarity solution $kE_n(k) \propto \mathrm{St}_r^2$ using the approximation $B \approx B_Q$ for $\tau_p \ll \tau_r$. Here, $\mathrm{St}_r \equiv \tau_p/\tau_r$ is the scale-dependent Stokes number [17,18,30] with $\tau_r = \epsilon^{-1/3}k^{-2/3}$ for a scale $r = k^{-1}$. Following K41, the representative velocity and pressure at the scale $k$ are scaled by $\epsilon^{1/3}k^{-1/3}$ and $\epsilon^{2/3}k^{-2/3}$ in the inertial subrange, respectively [20,25]. Then, we can expect $kE_n(k)$, $\tau_r kT(k)$ and $\tau_r kP_{\nabla\mathcal{P}}(k)$ to be given by a function of $\mathrm{St}_r$ even when the contribution of $B_\theta$ in $B_{\nabla\mathcal{P}} = B_Q + B_\theta$ is not negligible.

This expectation is verified by normalizing the spectra by a characteristic length $\Lambda \equiv \tau_p^{3/2}\epsilon^{1/2}$ [18] so that $k\Lambda = \mathrm{St}_r^{3/2}$, i.e., $\tau_r \sim \tau_p$ for $r \sim \Lambda$. The normalized spectra $E_n^\dagger(k\Lambda) \equiv E_n(k)/\Lambda$ and $T^\dagger(k\Lambda) \equiv \tau_r T(k)/\Lambda$ are displayed in Fig. 4. The spectra $E_n^\dagger(k\Lambda)$ in the inertial subrange, indicated by solid lines in Fig. 4(a), align on the same curve, which is a function of $k\Lambda$, for $\mathrm{Re}_\lambda = 648$ and $\mathrm{St} = 0.5$, 1.0, and 2.0. The spectra for $\mathrm{St} = 0.05$, 0.1, and 0.2 lay only near the curve. For the case of $\mathrm{Re}_\lambda = 402$, the spectra $E_n^\dagger(k\Lambda)$ in the inertial subrange do not show the alignment on the same curve because $Q$ and $\mathcal{P}$ do not obey the scaling predicted by the dimensional analysis [see Fig. 1(b)]. In Fig. 4(b), the transfer spectra $T^\dagger(k\Lambda)$ for $\mathrm{Re}_\lambda = 648$ align along a single curve in the inertial subrange more clearly for $0.05 \leq \mathrm{St} \leq 2.0$. These results support our conjecture that the spectra are given by a function of $\mathrm{St}_r$, whereas the slope of both spectra changes significantly depending on $k\Lambda$, i.e., $\mathrm{St}_r$. Therefore, the bump observed in $E_n(k)$ for $k\eta \lesssim 0.03$ for $\mathrm{St} \geq 0.5$ is due to the $\mathrm{St}_r$ dependence of $E_n^\dagger(k\Lambda)$ in the inertial subrange, which shows a negative slope for $k\Lambda \gtrsim 10^{-3}$ ($\mathrm{St}_r \gtrsim 10^{-2}$). The normalized production spectra $P_Q^\dagger(k\Lambda) \equiv \tau_r kP_Q(k)$, where $P_Q(k) \equiv 2\sum_k' \Re[\widehat{B_Q}(\boldsymbol{k})\hat{n}^*(\boldsymbol{k})]$, i.e., the contribution of the preferential concentration, are also displayed in

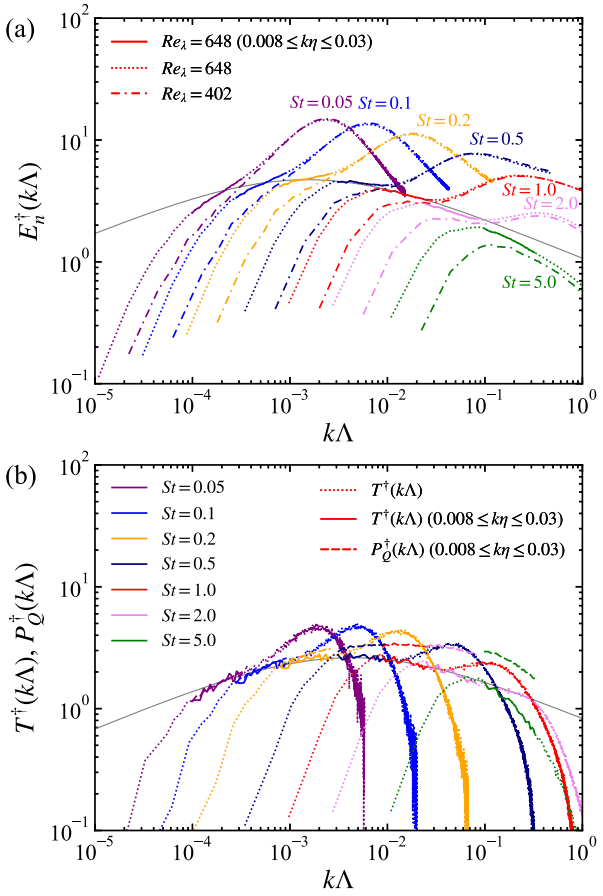


FIG. 4. (a) Normalized number density spectra $E_n^\dagger(k\Lambda)$ for $\mathrm{Re}_\lambda = 648$ and 402 and (b) normalized transfer spectra $T^\dagger(k\Lambda)$ for $\mathrm{Re}_\lambda = 648$. The spectra in the inertial subrange ($0.008 \lesssim k\eta \lesssim 0.03$) are indicated by the solid lines. The dashed lines in (b) are the normalized spectra $P_Q^\dagger(k\Lambda)$ for the production due to $B_Q$ for $\mathrm{Re}_\lambda = 648$ only in the inertial subrange. The gray solid lines in (a) and (b) are approximated functions for the inertial subrange, $E_n^\dagger(k\Lambda) \approx 82.1(k\Lambda)^{1/3}/(1+75.7\mathrm{St}_r)$ and $T^\dagger(k\Lambda) \approx 32.2(k\Lambda)^{1/3}/(1+37.8\mathrm{St}_r)$, respectively, where $k\Lambda = \mathrm{St}_r^{3/2}$.

Fig. 4(b), only in the inertial subrange. A clear discrepancy between $T^\dagger(k\Lambda)$ and $P_Q^\dagger(k\Lambda)$ can be observed for $k\Lambda \gtrsim 10^{-3}$, meaning that the clustering production for such scales is reduced by the contribution of $B_\theta$, i.e., the modulation due to the $n$ conservation. The observed $\mathrm{St}_r$ dependence of $E_n^\dagger(k\Lambda)$ implies that the spatial structure of $n$ at each scale changes depending on $\mathrm{St}_r$. It has been confirmed in the Supplemental Material [24] that the skewness and flatness factors at each scale of $n$ well exhibit the scale dependence as a function of $\mathrm{St}_r$.

If the $\mathrm{St}_r$ dependence of $E_n^\dagger(k\Lambda)$ holds even for higher $\mathrm{Re}_\lambda$, then we conjecture that the $\mathrm{St}_r$ dependence of the slope should be observed in the inertial subrange for $\mathrm{St} \gtrsim 0.5$. The Kolmogorov-like scaling predicted in Ref. [18] could be observed only for smaller values of $\mathrm{St}_r$, i.e., $\mathrm{St}_r \ll 10^{-2}$, supposing such a scaling exists. Assuming that the predicted scale similarity appears for $\mathrm{St}_r \ll 1$, $E_n^\dagger(k\Lambda)$ and

$T^{\dagger}(k\Lambda)$ can be approximated by functions. A least-square fitting of a rational function of the form $c_1/(1+c_2 St_r)$ with constants $c_1$ and $c_2$ to $(k\Lambda)^{-1/3}E_n^{\dagger}(k\Lambda)$ and $(k\Lambda)^{-1/3}T^{\dagger}(k\Lambda)$ in the inertial subrange results in the gray solid curves in Fig. 4. The curves well agree with the spectra for $\mathrm{St} \leq 2.0$ though the function form is chosen heuristically.

Experimental studies are also crucial to verify the scale dependence of the clustering for high Reynolds numbers. In Ref. [31], a plateau in the RDFs, referred to as a "shoulder region," was reported for $r/\eta \geq 50$ based on wind tunnel experiments for $\mathrm{Re}_\lambda$ up to 800. However, the authors stated that it was attributed to large-scale inhomogeneity caused by the experimental setup. Reference [32] reported that the clustering was observed up to the scales $300\eta$–$400\eta$ in experiments for $\mathrm{Re}_\lambda = 500$. In practical situations, e.g., laboratory experiments or cloud droplets and aerosols in the atmosphere, the gravitational settling further influences the clustering (e.g., Refs. [32–35]). Under the presence of gravity, the particle motion can be decoupled from the carrier turbulent flow. In the inertial subrange, the particle clustering would be modulated when the terminal velocity $v_T$ is larger than the flow velocity scale $u_r = \epsilon^{1/3}k^{-1/3}$ for a scale $k$. Therefore, for large scales that satisfy $v_T \ll u_r$, the settling effect could remain negligibly small as discussed in Ref. [36].

In this work, the pronounced inertial particle clustering has been discovered in the inertial subrange, in addition to the clustering in the near dissipation range. The obtained number density spectra well obey a function of $\mathrm{St}_r$ in the inertial subrange, showing a bump around $k\Lambda \approx 10^{-3}$. The clustering production is dominated by the preferential concentration mechanism for $k\Lambda \lesssim 10^{-3}$, whereas it is suppressed by the modulation due to the $n$ conservation for $10^{-3} \lesssim k\Lambda \lesssim 10^{-1}$. The discovered inertial particle clustering in the inertial subrange could have an impact on the subgrid-scale modeling for large-eddy simulations. The clustering of cloud droplets in the inertial subrange may also cause temperature and moisture fluctuations, which affect the condensation and evaporation of droplets in the raindrop formation process. Including the influence of gravitational setting, the spatial correlation for different Stokes numbers and turbulent mixing of clear air, in future work is important to understand and to model the droplet behavior in cloud turbulence.

K. M. acknowledges financial support from JSPS KAKENHI Grants No. JP20K04298 and No. JP23K03686. The direct numerical simulations presented here were conducted on the Earth Simulator supercomputer system operated by JAMSTEC.

*k.matsuda@jamstec.go.jp

[1] M. R. Maxey, The gravitational settling of aerosol particles in homogeneous turbulence and random flow fields, J. Fluid Mech. **174**, 441 (1987).
[2] K. D. Squires and J. K. Eaton, Particle response and turbulence modification in isotropic turbulence, Phys. Fluids A **2**, 1191 (1990).
[3] K. D. Squires and J. K. Eaton, Measurements of particle dispersion obtained from direct numerical simulations of isotropic turbulence, J. Fluid Mech. **226**, 1 (1991).
[4] R. A. Shaw, Particle-turbulence interactions in atmospheric clouds, Annu. Rev. Fluid Mech. **35**, 183 (2003).
[5] F. Toschi and E. Bodenschatz, Lagrangian properties of particles in turbulence, Annu. Rev. Fluid Mech. **41**, 375 (2009).
[6] R. Monchaux, M. Bourgoin, and A. Cartellier, Analyzing preferential concentration and clustering of inertial particles in turbulence, Int. J. Multiphase Flow **40**, 1 (2012).
[7] L. Brandt and F. Coletti, Particle-laden turbulence: Progress and perspectives, Annu. Rev. Fluid Mech. **54**, 159 (2022).
[8] J. Bec, K. Gustavsson, and B. Mehlig, Statistical models for the dynamics of heavy particles in turbulence, Annu. Rev. Fluid Mech. **56**, 189 (2024).
[9] R. Onishi and J. C. Vassilicos, Collision statistics of inertial particles in two-dimensional homogeneous isotropic turbulence with an inverse cascade, J. Fluid Mech. **745**, 279 (2014).
[10] P. J. Ireland, A. D. Bragg, and L. R. Collins, The effect of Reynolds number on inertial particle dynamics in isotropic turbulence. Part 1. Simulations without gravitational effects, J. Fluid Mech. **796**, 617 (2016).
[11] K. Matsuda, R. Onishi, M. Hirahara, R. Kurose, K. Takahashi, and S. Komori, Influence of microscale turbulent droplet clustering on radar cloud observations, J. Atmos. Sci. **71**, 3569 (2014).
[12] K. Matsuda and R. Onishi, Turbulent enhancement of radar reflectivity factor for polydisperse cloud droplets, Atmos. Chem. Phys. **19**, 1785 (2019).
[13] G. Boffetta, F. De Lillo, and A. Gamba, Large scale inhomogeneity of inertial particles in turbulent flows, Phys. Fluids **16**, L20 (2004).
[14] S. Goto and J. C. Vassilicos, Self-similar clustering of inertial particles and zero-acceleration points in fully developed two-dimensional turbulence, Phys. Fluids **18**, 115103 (2006).
[15] H. Yoshimoto and S. Goto, Self-similar clustering of inertial particles in homogeneous turbulence, J. Fluid Mech. **577**, 275 (2007).
[16] R. Monchaux, M. Bourgoin, and A. Cartellier, Preferential concentration of heavy particles: A Voronoï analysis, Phys. Fluids **22**, 103304 (2010).
[17] A. D. Bragg, P. J. Ireland, and L. R. Collins, Mechanisms for the clustering of inertial particles in the inertial range of isotropic turbulence, Phys. Rev. E **92**, 023029 (2015).
[18] T. Ariki, K. Yoshida, K. Matsuda, and K. Yoshimatsu, Scale-similar clustering of heavy particles in the inertial range of turbulence, Phys. Rev. E **97**, 033109 (2018).
[19] S. Oka and S. Goto, Generalized sweep-stick mechanism of inertial-particle clustering in turbulence, Phys. Rev. Fluids **6**, 044605 (2021).
[20] A. N. Kolmogorov, The local structure of turbulence in incompressible viscous fluid for very large Reynolds numbers, Dokl. Akad. Nauk SSSR **30**, 299 (1941); reprinted in Proc. R. Soc. A **434**, 9 (1991).

[21] R. Onishi, Y. Baba, and K. Takahashi, Large-scale forcing with less communication in finite-difference simulations of steady isotropic turbulence, J. Comput. Phys. **230**, 4088 (2011).
[22] K. Matsuda, K. Schneider, and K. Yoshimatsu, Scale-dependent statistics of inertial particle distribution in high Reynolds number turbulence, Phys. Rev. Fluids **6**, 064304 (2021).
[23] K. Yoshida and T. Arimitsu, Inertial-subrange structures of isotropic incompressible magnetohydrodynamic turbulence in the Lagrangian renormalized approximation, Phys. Fluids **19**, 045106 (2007).
[24] See Supplemental Material at http://link.aps.org/supplemental/10.1103/PhysRevLett.132.234001 for sensitivity to external forcing schemes, computation of the number density spectrum, compensated number density spectrum, and scale dependence of skewness and flatness factors for number density.
[25] A. S. Monin and A. M. Yaglom, *Statistical Fluid Mechanics* (MIT Press, Cambridge, MA, 1975), Vol. 2.
[26] T. Gotoh and D. Fukayama, Pressure spectrum in homogeneous turbulence, Phys. Rev. Lett. **86**, 3775 (2001).
[27] T. Ishihara, Y. Kaneda, M. Yokokawa, K. Itakura, and A. Uno, Spectra of energy dissipation, enstrophy and pressure by high-resolution direct numerical simulations of turbulence in a periodic box, J. Phys. Soc. Jpn. **72**, 983 (2003).
[28] I. Saito and T. Gotoh, Turbulence and cloud droplets in cumulus clouds, New J. Phys. **20**, 023001 (2018).
[29] K. Matsuda, K. Yoshimatsu, and K. Schneider, Large-scale clustering of inertial particles in homogeneous isotropic turbulence, *Proceedings of 12th International Symposium on Turbulence and Shear Flow Phenomena* (2022), http://www.tsfp-conference.org/proceedings/2022/341.pdf.
[30] J. Bec, L. Biferale, M. Cencini, A. Lanotte, S. Musacchio, and F. Toschi, Heavy particle concentration in turbulence at dissipative and inertial scales, Phys. Rev. Lett. **98**, 084502 (2007).
[31] E.-W. Saw, R. A. Shaw, J. P. L. C. Salazar, and L. R. Collins, Spatial clustering of polydisperse inertial particles in turbulence: II. Comparing simulation with experiment, New J. Phys. **14**, 105031 (2012).
[32] A. J. Petersen, L. Baker, and F. Coletti, Experimental study of inertial particles clustering and settling in homogeneous turbulence, J. Fluid Mech. **864**, 925 (2019).
[33] J. Bec, H. Homann, and S. S. Ray, Gravity-driven enhancement of heavy particle clustering in turbulent flow, Phys. Rev. Lett. **112**, 184501 (2014).
[34] K. Gustavsson, S. Vajedi, and B. Mehlig, Clustering of particles falling in a turbulent flow, Phys. Rev. Lett. **112**, 214501 (2014).
[35] P. J. Ireland, A. D. Bragg, and L. R. Collins, The effect of Reynolds number on inertial particle dynamics in isotropic turbulence. Part 2. Simulations with gravitational effects, J. Fluid Mech. **796**, 659 (2016).
[36] J. Lu, H. Nordsiek, and R. Shaw, Clustering of settling charged particles in turbulence: Theory and experiments, New J. Phys. **12**, 123030 (2010).